Title: A peptide that regulates metalation and function of the *Arabidopsis* ethylene receptor

Authors:
Anna J. Mudge[1]†, Saher Mehdi[1]††, Will Michaels[1,2]†, Beatriz Orosa-Puente[1]‡, Weiran Shen[1], Ari Sadanandom[1], Flora M. Hetherington[1]‡‡, Claudia Hoppen[3], Buket Uzun[3], Georg Groth[3], Jennifer F. Topping[1], Nigel J. Robinson[1,2*], Keith Lindsey[1*]

Affiliations:
[1]*Department of Biosciences, Durham University, Durham, UK*
[2]*Department of Chemistry, Durham University, Durham, UK*
[3]*Institute of Biochemical Plant Physiology, Heinrich Heine University Düsseldorf, D-40204 Düsseldorf, Germany*

†These authors contributed equally to this work
††Present address: wellOwise Research and Development, IIITD Innovation & Incubation Centre, New Delhi, Delhi - 110020, India.
‡Present address: School of Biological Sciences, University of Edinburgh, Edinburgh EH9 3FF, UK.
‡‡Present address: University of Bath, Claverton Down, Bath BA2 7AY, U.K.
*Joint corresponding authors: keith.lindsey@durham.ac.uk; nigel.robinson@durham.ac.uk

Abstract:
Ethylene signalling represents one of the classic hormonal pathways in plants, with diverse roles in development and stress responses. The dimeric ethylene receptor localizes to the endoplasmic reticulum (ER) and contains Cu(I) ions essential for ethylene binding and signalling. As for other vesicular cupro-proteins, the final step of Cu(I) maturation at the ER is undefined. We previously discovered that mutants in the *Arabidopsis* gene *POLARIS* (*PLS*), encoding a 36 amino acid peptide, exhibit constitutive ethylene signalling responses. Here we report a 1:2 thiol-dependent Cu(I):PLS_2 complex, with an affinity of 3.79 (±1.5) x10^{19} M^{-2}. We demonstrate PLS interactions with the transmembrane domain of receptor protein ETR1, the Cu(I) chaperones ATX1 and CCH, and Cu(I)-transporting P_{1B}-type ATPase RAN1 at the ER. Formation of Cu(I)-dependent PLS-cuproprotein adducts at the ER provides a mechanism to modulate the metalation of ETR1, thereby regulating its activity and representing a novel mechanism for plant hormone receptor regulation.

One Sentence Summary: The POLARIS peptide of *Arabidopsis* regulates activity of the ethylene hormone receptor by controlling Cu(I) availability.

Main text

Ethylene is used by plants as a gaseous hormone to regulate many aspects of development and responses to biotic and abiotic stresses (*1*). It is perceived by a family of receptors that, in *Arabidopsis*, comprises 5 members, ETR1 (ETHYLENE RESPONSE 1), ERS1 (ETHYLENE RESPONSE SENSOR 1), ERS2, ETR2, and EIN4 (ETHYLENE-INSENSITIVE 4) (*2-5*) located on the endoplasmic reticulum (ER) (*6, 7*). The receptors are related to bacterial two-component systems (*2*), form dimers through disulphide bonding at the N-terminal hydrophobic domains (*8, 9*) and contain Cu(I) ions bound to residues Cys65 and His69, essential for ethylene binding and

signal transduction (*10, 11*). In the absence of ethylene these receptors activate a negative regulator CTR1 (CONSTITUTIVE TRIPLE RESPONSE 1), a mitogen-activated protein kinase kinase kinase (MAPKKK), so preventing ethylene responses (*12, 13*). Mechanisms by which receptor activity is regulated are not well understood. We describe here a molecular mechanism of the PLS peptide, and a proposed model for its role in plant development.

Introduction of copper to the ER and ethylene receptor requires the RAN1 (RESPONSIVE TO ANTAGONIST1) protein. This is a predicted copper-transporting P-type ATPase homologous to the yeast Ccc2p and to human Menkes and Wilson disease proteins (*14*). Strong loss-of-function mutants of *RAN1* in *Arabidopsis* (e.g. *ran1-3*, *ran1-4*) exhibit a constitutive ethylene signalling response (*15*), consistent with a loss of receptor function, and similar to higher order loss-of-function receptor mutants, which also show an ethylene hypersignalling phenotype (*16*). Mechanisms of copper homeostasis, post-RAN1 but pre-ETR1, are unknown, and indeed this is true for other compartmentalized cuproproteins supplied with copper, for example via Ccc2p, Menkes or Wilson ATPases.

Results

The POLARIS peptide is a negative regulator of ethylene responses

The *POLARIS* gene of *Arabidopsis* (AT4G39403) encodes a 36 amino acids peptide (Fig. 1a) that, in light-grown seedlings, is most strongly expressed in the root tip and vascular tissues (*17*). We have previously shown that the loss-of-function *pls* mutant is phenotypically similar to *ran1* loss-of-function alleles and *ctr1*, exhibiting a triple response phenotype (short hypocotyl and root, exaggerated apical hook, radial expansion) in the dark in the absence of ethylene (*18*), and a short root in light-grown seedlings (Fig. 1b). Transgenic complementation of the mutant and overexpression of the *PLS* gene suppresses the mutant phenotype, but fails to suppress the *ctr1* mutant phenotype, indicating that the PLS peptide acts upstream of CTR1 (*18*). The *pls* mutant phenotype is rescued by the gain-of-function ethylene resistant mutation *etr1-1* and pharmacological inhibition of ethylene signalling by silver ions (*18*). Ethylene gas production in the *pls* mutant is at wildtype levels, indicating the peptide plays a role in ethylene signalling rather than biosynthesis (*18*). RNA-seq on loss-of-function *pls* mutant and gain-of-function *PLS* transgenic overexpressor (PLSOx) seedlings shows that the *pls* mutant expresses no full length PLS coding sequence, while the PLSOx seedlings express ca. 18-fold higher levels of *PLS* transcript compared to wild-type (Fig. S1; Table S1). Gene Ontology (GO) analysis following RNA-seq transcriptomics of *pls* mutant seedlings shows the up-regulation of genes associated with responses to hormone signalling, biotic and abiotic defence responses, and cell death (Table S1; Fig. S2a). Eighty-four of 353 known ethylene-related genes are significantly up-regulated in the *pls* mutant compared to wildtype, and genes down-regulated in *pls* include categories associated with root morphogenesis, root epidermal cell differentiation, hormone biosynthetic processes, response to nutrients and metal ion transport (Fig. S2; *19*). In PLSOx overexpressors, up-regulated genes include those associated with hormone responses, biotic and abiotic stress responses and cell death; while 169 of 1615 genes associated with response to hormone stimulus are down-regulated compared to wildtype (Fig. S2c, d; *19*). Genes associated with metal ion transport are also down-regulated in PLSOx seedlings (Fig. S2d; *19*). Twenty-four ethylene-related genes are both up-regulated in the *pls* mutant and down-regulated in the PLS-overexpressor, compared with wild-type (Fig. 1c; *19*). This is consistent with a role for PLS in ethylene responses and other, potentially related, signalling, stress and developmental processes.

To further understand the relationship between PLS peptide structure and function, and to investigate conservation of PLS function between species, we carried out synthetic peptide

feeding experiments using hydroponically grown seedlings. The *Arabidopsis* relative *Camelina sativa* contains a gene with partial sequence identity to the *Arabidopsis PLS* gene, encoding a predicted peptide sequence that is 22 amino acids long and identical to the N-terminal 22 amino acids of the *Arabidopsis* PLS except for a phenylalanine to serine substitution at position nine (Fig. 1a). We synthesized full-length PLS peptide, PLS(FL) and truncated versions from both *Arabidopsis* and *C. sativa* (Fig. 1a), and supplied the peptides to *Arabidopsis pls* mutant seedlings hydroponically. The full-length peptides from both *Arabidopsis* and *C. sativa* were each able to rescue the short primary root length of the *Arabidopsis pls* mutant (Fig. 1D), similar to transgenic overexpression and genetic complementation (*17, 18*). PLS(FL) peptide effects on root growth appear to be dose-dependent, as indicated both by genetic studies (*17*) and peptide feeding (Fig. S3a). However, neither a 9 amino acids sequence (N2, Fig. 1e) from the N-terminus, nor C-terminal sequences of 14 (C1) or 24 (C2) amino acids from *Arabidopsis* PLS were able to rescue the mutant (Fig. 1e). Imaging showed that a fluorescent tagged (5-carboxyfluorescein, 5-FAM) version of the *Arabidopsis* N-terminal 22 amino acids sequence of the peptide (N1) is taken up by the roots, and also rescues the mutant root phenotype (Fig. S3b, c).

PLS localizes to the endoplasmic reticulum

Since genetic studies suggest that PLS acts close to the ethylene receptor (*18*), we hypothesized that it should localize to the same subcellular compartment. The ethylene receptor in *Arabidopsis* is localized to the ER (*12*), and ER localization of a proPLS::PLS:GFP fusion protein was confirmed by co-localization with the ER marker dye ER-Tracker™ (Fig. 2a-c) and with an ER-targeted red fluorescent protein RFP-HDEL (*20*) in transgenic plants (Fig. 2g-i). proPLS::PLS:GFP also appears to localize to the nucleus (Fig. 2). As controls, free GFP protein expressed under the control of the PLS promoter is not co-localized to the ER (Fig. 2d-f) and, as expected, the Golgi marker SH:GFP does not co-localize with ER Tracker (Fig. 2m-o). *Trans*-Golgi-localized SULFOTRANSFERASE1 (ST1) mCherry (*21*) show proPLS::PLS:GFP does not localize to the Golgi (Fig. 2j-l). To further clarify the side of the ER membrane on which PLS localizes, transient expression of redox-sensitive GFP (roGFP2) fusions of PLS were carried out. The different excitation properties of roGFP2 in an oxidizing (ER lumen) or reducing environment (cytosol) allows discrimination of the precise location of PLS. Ratiometric analysis and comparison with proteins of known localization revealed that PLS resides at the cytosolic side of the ER and is not localized in the ER lumen (Fig. 2p).

PLS interacts with the ethylene receptor protein ETR1

We hypothesized that PLS plays a role in receptor function and investigated whether this involved direct interaction with the receptor complex. Preliminary experiments using yeast 2-hybrid analysis suggested that PLS interacts with ETR1 (Fig. S4). Confirmation of the physical interaction between PLS and ETR1 in plants came from co-immunoprecipitation (Co-IP) analysis. *Agrobacterium* containing a plasmid encoding PLS linked to a C-terminal GFP and ETR1 with a C-terminal HA tag was infiltrated into *Nicotiana benthamiana* leaves for transient expression. After 3 d, interaction was confirmed by western blotting after Co-IP with either anti-GFP beads (showing PLS pulls down ETR1) or anti-HA beads (showing ETR1 pulls down PLS) (Fig. 3a). GFP-only controls did not show binding with ETR1, demonstrating the interaction is dependent on the presence of the PLS peptide.

The addition of 0.5 μM copper sulphate to the protein extract used for Co-IP experiments stabilized the PLS-ETR1 interaction. The presence of copper ions resulted in almost 3-fold more PLS:GFP detected upon pulldowns with ETR1-HA, or conversely of ETR1-HA pulled down with PLS-GFP, compared to the same assay in the presence of the metal chelator 2 mM EDTA

143 (Fig. 3a, b).
144 To investigate the specificity of PLS binding, synthetic full length PLS peptide PLS(FL) was
145 introduced into the infiltrated *N. benthamiana* leaves 30 min before the tissue was harvested. The
146 addition of 25 nM synthetic PLS caused a ca. 80% reduction in PLS-GFP binding to ETR1-HA
147 (Fig. 3c, d), suggesting that the synthetic PLS peptide competes for ETR1 binding, and showing
148 the specificity of PLS for ETR1. Interestingly, the anti-GFP beads bound two sizes of PLS-GFP
149 protein (Fig. 3e), both of which were larger than a GFP-only control, suggesting that the PLS
150 peptide undergoes cleavage, a change in conformation, post-translational modification or
151 incomplete reduction of Cys residues on some PLS. When using ETR1-HA to pull down PLS-
152 GFP, only the larger peptide was present (Fig. 3e, f), suggesting that ETR1 binds the full length
153 PLS peptide, but that PLS may be modified after ETR1 binding.
154 To pinpoint the interaction site at the receptor in more detail, binding studies were performed
155 with purified receptor variants and PLS by microscale thermophoresis (MST; Fig. 3g). Binding
156 of PLS was observed only with receptor variants containing the N-terminal transmembrane
157 domain (TMD). In contrast, no binding was detected with ETR1 lacking this domain ($ETR1^{306-}$
158 ^{738}). The TMD harbors the ethylene and copper binding region (*22*).
159
160 **PLS binds Cu(I) and forms protein adducts with copper chaperones ATX and CCH and**
161 **with RAN1**
162 Cysteine residues are common metal-ligand binding residues in low molecular weight copper-
163 handling peptides, and predictions of PLS structure suggests a single α-helix plus unstructured
164 region with two cysteines ($CX_{10}C$ arrangement where X is any amino acid), with some analogy
165 to copper-metallochaperones such as Cox17 or other CX_9C twin proteins (*23*). In view of both
166 structural considerations and the copper-dependency of ETR1 we determined whether the two
167 cysteine residues (C6 and C17) in PLS play a functional role, such as in copper binding. A
168 mutated *Arabidopsis* full-length peptide in which both cysteines were replaced with serine,
169 PLS(FL C6S, C17S), was non-functional in root feeding assays (Fig. 4a), indicating the
170 importance of the cysteine residues for biological activity. To determine a possible role for PLS
171 in binding Cu(I), we first grew *pls* mutants and wildtype seedlings in the presence of the copper
172 chelator bathocuproine disulphonic acid (BCS), which is often used to deplete copper but notably
173 solubilises and stabilises Cu(I). Treatment of *pls* and wildtype seedlings with 10 µM and 50 µM
174 BCS led to an increased primary root length of both genotypes, while 100 µM BCS led to
175 significantly enhanced root growth in the *pls* mutant compared with wildtype (Fig. 4b); and
176 rescue of the overexpression of ethylene-responsive genes (Fig. S5; *19*). This suggests that the
177 availability of Cu(I) is growth-limiting in the *pls* mutant through abnormal ethylene perception.
178 Bicinchoninic acid (BCA) is a chromophore that binds Cu(I) (*24*) (Fig. 4c and S6). Titration
179 experiments show that synthetic PLS(FL) withholds Cu(I) from BCA (Fig. S7), but the mutant
180 PLS (FL C6S, C17S) does not (Fig. S8). Attempts to determine the stoichiometry and affinity
181 for Cu(I) were confounded by precipitation of the synthetic peptide, whereas PLS fusion to
182 maltose binding protein (MBP-PLS) retained solubility when titrated with Cu(I) ions under
183 strictly anaerobic conditions. MBP-PLS (14 µM) withholds ca. 7 µM Cu(I) from BCA, indicative
184 of a 2:1 PLS:Cu(I) stoichiometry, and tight binding is cysteine-dependent (Fig. 4d). A β_2 affinity
185 of 3.79 (±1.5) $x10^{19}$ M^{-2} was determined by competition against an excess of BCA, and the fit
186 significantly departs from simulations 10x tighter or weaker (Fig. 4e, Fig. S9).
187 Metal binding in biology is challenging to predict because the formation of metal-protein
188 complexes is a combined function of metal affinity for a given protein and metal availability,
189 which would need to be known for Cu(I) in the *Arabidopsis* cytosol in the case of PLS (Fig. 2p).
190 Cu(I) occupancy of the cytosolic copper chaperone ANTIOXIDANT PROTEIN 1 (ATX1) tracks

with fluctuations in available cytosolic Cu(I) such that its affinity approximates to the mid-point of the range of Cu(I) availabilities within this eukaryotic compartment (*25, 26*). *Arabidopsis* ATX1 was therefore expressed and purified to determine a 1:1 ATX1:Cu(I) stoichiometry and affinity $K_{D\ Cu(I)}$ of 5.47 (±0.6) x10^{-18} M (Fig. 4f inset, Fig. S10). Figure 4f (main panel) reveals that the cytosolic concentration of PLS would need to exceed (improbable) millimolar concentrations for Cu(I)-dependent homodimers to form at this cytosolic Cu(I) availability (mathematical models and equations shown in Supplementary text). It is thus unlikely that the Cu(I):PLS_2 complex alone delivers Cu(I) to interacting cuproprotein ETR1. Cu(I)-dependent PLS heterodimeric adducts are the more likely functional species.

Together these results suggest a model in which PLS is involved in the RAN1-dependent maturation of Cu(I)ETR1 at the ER. To investigate possible interaction between PLS and RAN1, PLS was titrated to fluorescently labelled RAN1 and RAN1 truncation mutants. RAN1, NterRAN1 and CterRAN1 were purified and labelled as described (*27*). NterRAN1 is a truncation containing only the two N-terminal metal-binding-domains, whereas CterRAN1 is a construct lacking this region. Using Microscale Thermophoresis, direct interaction was observed between PLS and RAN1. Dissociation constants indicate that PLS interacts predominantly with the N-terminal metal-binding-domains, but only weakly with the C-terminal region (Fig. 4g). Moreover, the soluble copper chaperones ATX1 and CCH also interact with PLS. Titration experiments were carried out with fluorescently labelled copper chaperones ATX1, CCH and CCHΔ, a mutant lacking the plant specific C-terminal extension. PLS interacts with these soluble copper chaperones at similar affinity as obtained for RAN1 (Fig. 4h). Of relevance here is the observation that ATX1 interacts directly with RAN1 to deliver copper at the ER (*28*). Cu(I)-dependent PLS heterodimeric adducts may therefore modulate multiple cuproproteins in the Cu(I)ETR1 maturation pathway.

The formation of PLS adducts with otherwise unsaturated copper coordination spheres, can inhibit the formation of aberrant copper-bridged complexes during metalation or during re-organisation of copper sites. This can, in turn, influence the rate of holo-ETR1 maturation, plus potentially the rates of ETR1 deactivation and reactivation. In this model, a down-regulation of *PLS* or loss-of-function mutation of the *PLS* gene leads to a depletion of correctly coordinated Cu(I) at the receptor through reduced intermediate PLS heterodimer adduct formation, in turn leading to a non-functional receptor that cannot activate CTR1, with a consequent activation of ethylene signaling, similar to *ran1* or *etr1* loss-of-function mutants, and/or through the effect of ethylene on reducing *PLS* expression (Figs. S11, S12). Overexpression of PLS phenocopies the ethylene-insensitive *etr1-1* gain-of-function mutant (*18*), presumably by a conformational change in the receptor on binding, to promote a functional interaction with CTR1 and suppressing ethylene responses. The PLS complex may be removed from ETR1 by dissociation of a PLS-ETR1-RAN1-chaperone complex following ligand-exchange, and/or modulated by PLS modification or cleavage. It is speculated that similar PLS-dependent events may also be required to re-set the receptor, perhaps following changes in the copper coordination sphere coincident with gain or loss of cation-π bonds between copper and ethylene. Hormonal regulation of *PLS* expression forms a signaling network to regulate ethylene responses and root growth with other hormones, such as by its activation to suppress growth-inhibitory ethylene responses in the high auxin environment of the root tip (*29*) (Fig. S12). Future structural studies should reveal more about the PLS-adduct-receptor interaction and role of copper ions in ethylene signal transduction, which represents a new paradigm for the regulation of signaling protein function by metals.

238 # Methods

239 **Plant Material**

240 Seedlings of *Arabidopsis thaliana* ecotype either C24 or Col-0, or *pls* mutants or transgenic *PLS*
241 overexpressers, all from lab stocks, were grown on solid sterile half-strength MS10 medium on
242 2.5% Phytagel (Sigma-Aldrich) in 90 mm Petri dishes (Sarstedt, Leicester, UK) at 21°C, under
243 a 16 hour photoperiod as described (*17, 18*). *Nicotiana benthamiana* plants (lab stocks) were
244 grown in a controlled environment (21°C, 16 h photoperiod) for transient expression studies in
245 leaf tissue. For hydroponic feeding studies, *Arabidopsis* seedlings were cultured in liquid
246 medium (1 ml/well) in sterile 24-well plates (Sarstedt), essentially as described (*30*). For
247 hormone and peptide assays, one seedling was grown in each well, at 21°C, under a 16 h
248 photoperiod. For peptide feeding experiments, purified freeze-dried peptide was dissolved in
249 DMSO to create a 500 µM stock solution. Peptide stock solution was added to liquid ½ MS10
250 plant media containing 0.1% DMSO to make a final peptide concentration of 50 or 100 nM (or
251 10, 25, 50 and 100 nM for dose-dependent assays). For copper treatments, 1 mM $CuSO_4$ solution
252 was filter-sterilized and added to autoclaved liquid ½ MS10 plant media to create final $CuSO_4$
253 concentrations of 0, 5, 10, 15, 20, 25, 30, 35, 40, 45 and 50 µM. The copper chelator
254 bathocuproine disulphonic acid (BCS) was added to liquid medium to produce final
255 concentrations of 0, 10, 50, 100, 250 and 500 µM. Seedlings were scanned to create a digital
256 image and root lengths of seedlings were measured using ImageJ. Statistical analysis was
257 performed using the Real Statistics Resource Pack software (Release 3.8, www.real-
258 statistics.com) in Excel (Microsoft).
259

260 **Peptide Synthesis**

261 Peptides were either obtained from Cambridge Research Biochemicals (Billingham, UK) or
262 synthesized in the laboratory by Fmoc solid phase peptide synthesis (SPPS) on a CEM Liberty1
263 single-channel peptide synthesiser equipped with a Discover microwave unit. Reactions were
264 performed in a 30 ml PTFE reaction vessel with microwave heating and agitation by bubbling
265 nitrogen. Peptide synthesis was carried out using 2-chlorotrityl chloride resin (0.122 mmol g^{-1},
266 Novabiochem) using Fmoc-protected amino acids. The first amino acid residue at the C-terminus
267 (histidine) was coupled manually by mixing 76 mg (1 eq.) Fmoc-His(Trt)-OH, 0.09 ml (4 eq.)
268 *N,N*-diisopropylethylamine (DIPEA), 1 ml dichloromethane (DCM) and 1 ml
269 dimethylformamide (DMF) until the amino acid powder had dissolved. The mixture was added
270 to 0.1 mmol resin and stirred gently for 120 minutes at room temperature. Resin was washed
271 with 3x DCM/MeOH/DIPEA (17:2:1), 3x DCM, 2x DMF and 2x DCM. Amino acid coupling
272 reactions were performed using Fmoc-protected amino acids present in a 5-fold excess (2 M
273 concentration), HOBt (0.5 M HOBt in DMF, used at the activator position) and DIC (0.8 M in
274 DMSO, used at the activator base position). For double and triple couplings the reaction vessel
275 was drained after each coupling cycle and fresh reagents were added. Before each coupling, a
276 room temperature preactivation period of 1 to 2 hours was used. Microwave-assisted couplings
277 were performed for 10 minutes at 75°C at 25W power. Cys and His residues were coupled at low
278 temperature (10 minutes at room temperature followed by 10 minutes at 50°C, 25W). Arg
279 residues were double coupled, firstly by 45 minutes at room temperature plus 5 minutes at 75°C
280 (25W), and second by the standard microwave conditions above. Fmoc group removal was
281 carried out by two piperidine solution treatments (20% piperidine in DMF) in succession: 5
282 minutes then 10 minutes. Peptide cleavage from resin was carried out in 3 ml 95% TFA in dH^-
283 $_2O$/TIPS (2.85 ml TFA, 0.15 ml dH_2O, 0.15 ml triisopropylsilane). Peptide was dissolved in water

284 with a small volume of MeCN and lyophilized to produce a powder using a Christ ALPHA 1-2
285 LD_{plus} freeze dryer.
286
287 **Preparative High-Performance Liquid Chromatography (HPLC)**
288 Peptide products were analysed and purified by HPLC at 280 nm. 25-50 mg of freeze-dried
289 peptide sample was dissolved in 1 ml 1:1 H_2O:MeCN and injected onto a Speck and Burke
290 Analytical C18 Column (5.0 µm, 10.0 x 250 mm) attached to a PerkinElmer (Massachusetts,
291 USA) Series 200 LC Pump and 785A UV/Vis Detector. Separation was achieved by gradient
292 elution of 10-80% solvent B (solvent A = 0.08% TFA in water; solvent B = 0.08% TFA in ACN)
293 over 60 minutes, followed by 80-100% B over 10 minutes, with a flow rate of 2 ml/min. Selected
294 peptide fractions were lyophilized and a mass assigned using MALDI-TOF MS. Peptide
295 sequences were identified using MALDI-TOF MS, using an Autoflex II ToF/ToF mass
296 spectrometer (Bruker Daltonik GmBH, Germany) equipped with a 337 nm nitrogen laser. MS
297 data was processed using FlexAnalysis 2.0 (Bruker Daltonik GmBH).
298
299 **Imaging**
300 CSLM images were obtained by a Leica SP5 TCS confocal microscope using 40X and 63X oil
301 immersion lenses. For propidium iodide staining, whole *Arabidopsis* seedlings were incubated
302 in 10 mg/l propidium iodide solution for 90 s. *pPLS::PLS:GFP, pPLS::GFP* and *p35S::GFP*
303 seedlings were grown for 7 d on Phytagel ½ MS10 medium before ca. 25 mm of the root tip was
304 removed and mounted in dH_2O on a microscope slide, and a 1.5 mm cover slip was placed on
305 top prior to imaging. The ER marker p35S::RFP:HDEL (*20*) (kindly provided by Dr. Pengwei
306 Wang, Durham University), and the trans-Golgi apparatus marker *pFGC-ST:mCherry* (obtained
307 from Nottingham Arabidopsis Stock Centre, www.arabidopsis.info) were introduced into
308 *pPLS::PLS:GFP* plants by the floral dip method of transformation (*31*) using *A. tumefaciens*
309 GV3 101. ER was also localized using ER Tracker™ Red (Life Technologies). Seven day-old
310 seedlings were stained for 30 min in the dark in liquid ½ MS10 media containing 1 µM ER
311 Tracker™ Red.
312
313 **RNA Isolation, RNA Sequencing, RT-qPCR**
314 RNA was extracted from 7 day-old seedlings grown on half strength MS10 medium using the
315 Sigma-Aldrich Plant Total RNA Kit (STRN50) and the On-Column DNase I Digestion Set
316 (DNASE10-1SET), essentially as described (*32*). Tissue was ground in liquid nitrogen before
317 incubation in lysis solution containing 2-mercaptoethanol at 65°C for 3 min. Debris was removed
318 by centrifugation and column filtration and RNA was captured onto a binding column using the
319 supplied binding solution. DNA was removed by wash solutions and DNase treatment on the
320 column. Purified RNA was eluted using RNAase free water.
321 The Illumina HiSeq 2500 System was used for RNA sequencing of three biological replicate
322 samples, with libraries prepared using the Illumina TruSeq Stranded Total RNA with Ribo-Zero
323 Plant Sample Preparation kit (RS-122-2401), essentially as described (*32*). Ribosomal RNA
324 (rRNA) was removed and purified RNA was quality checked using a TapeStation 2200 (Agilent
325 Technology) with High Sensitivity RNA ScreenTape (5067-5579). mRNA was fragmented into
326 120-200 bp sequences with a median size of 150 bp, and used as template to synthesize first
327 strand cDNA using reverse transcriptase and random primers, followed by second strand cDNA
328 synthesis with DNA Polymerase I and RNase H. Newly synthesized cDNA had a single adenine
329 base added with ligation of adaptors, before being purified and amplified by PCR to make the
330 final library. Library quality control was carried out again using a TapeStation with D1000
331 ScreenTape (catalog number 5067-5582). RNA-seq data were processed and aligned against the

332 TAIR10 (EnsemblePlants) genome using TopHat and indexed with Samtools. DeSeq determined
333 differential expression. A padj-value of ≤ 0.05 and a $\log_2$fold change ($\log_2$FC) of ≥ 0.5 were
334 selected to identify differentially expressed genes (DEGs). RNA-seq data are deposited in the
335 Dryad Digital Repository (*19*).
336 For RT-qPCR, RNA was extracted from 7 day-old seedlings (3 biological replicates, 20 mg of
337 tissue) as described (*32*). Total mRNA was extracted using Dynabeads®mRNA DIRECT™kit
338 with Oligo$(dT)_{25}$ labelled magnetic beads. cDNA was prepared using a SuperScript®IV First-
339 Strand synthesis system. Samples were checked for the presence of genomic DNA by PCR with
340 *ACTIN2* primers ACT2 forward and reverse. Primer sequences were determined using Primer-
341 BLAST (https://www.ncbi.nlm.nih.gov/tools/primer-blast/). Primers are listed in Table S2.
342
343 **Protein-protein interaction studies**
344 **Yeast 2-hybrid**
345 The GAL4 two-hybrid phagemid vector system was used to detect protein-protein interactions
346 *in vivo* in yeast, using the reporter genes β-galactosidase *(lacZ)* and histidine (*HIS3*) in the YRG-
347 2 yeast strain, essentially as described (*34*). DNA that encodes the target (ETR1) and bait (PLS)
348 was inserted into the pAD-GAL4-2.1 A and pBD-GAL4 Cam phagemid vectors respectively and
349 expressed as hybrid protein. The hybrid proteins were then assayed for protein-protein
350 interaction.
351 DNA encoding the target and bait proteins were prepared by PCR amplification using primer
352 designed the specifically for the DNA encoding the target (ETR1) and bait (PLS). Each set of
353 primer contained specific endonucleases on the ends of primer corresponding to the
354 endonucleases in the MCS of pAD-GAL4-2.1 A and pBD-GAL4 Cam phagemid vectors. The
355 DNA construct of the target (ETR1) and bait (PLS) with specific restriction sites on the ends was
356 then transformed into the TOPO 2.1 vector to check the sequence of the amplified DNA by
357 sequencing with M13 forward (CTG GCC GTC GTT TTA C) and M13 reverse (CAG GAA
358 ACA GCT ATG AC). The two vectors, pAD-GAL4-2.1 and pBD-GAL4 Cam were digested
359 using specific restriction endonucleases and dephosphorylated prior to ligating the insert DNA.
360 The DNA encoding the target (ETR1) and bait (PLS) was then ligated into the same reading
361 frame as the GAL4 AD of the pAD-GAL4-2.1 phagemid vector and the GAL4 BD of the pBD-
362 GAL4 Cam phagemid vector.
363 The following primers were used for PCR amplification:
364 ETR1:
365 Forward primer GAA TCC ATG GAA GTC TGC AAT TGT A (Eco RI on 5' end)
366 Reverse primer GTC GAC TTA CAT GCC CTC GTA CA (Sal I on 5'end)
367 PLS:
368 Forward primer CTG GAG ATG AAA CCC AGA CTT TGT (Xho I on 5' end)
369 Reverse primer GTC GAC ATG GAT TTT AAA AAG TTT (Sal I on 5' end)
370 The pGAL4 control plasmid was used alone to verify that induction of the *lacZ* and *HIS3* genes
371 has occurred and that the gene products are detectable in the assay used. The pLamin C control
372 plasmid was used in pairwise combination with the pAD-WT control plasmid or with the pAD-
373 MUT control plasmid to verify that the *lacZ* and *HIS3* genes are not induced as the protein
374 expressed by each of these pairs do not interact *in vivo*.
375 The control plasmids were transformed into the YRG-2 strain prior to the initial transformation
376 of the bait and the target plasmids. The control plasmids were used separately or in pairwise
377 combination in the transformation of the YRG-2 yeast strain. The yeast competent cells were
378 cotransformed with the bait and target plasmids by sequential transformation. First, yeast were

379 transformed with the bait plasmid and assayed for expression of reporter genes. Second, yeast
380 competent cells containing the bait were prepared and transformed with the target plasmid.
381
382 **Bimolecular fluorescence complementation analysis (BiFC)**
383 BiFC was carried out essentially as described previously (*35*). Full-length *Arabidopsis* ETR1 and
384 PLS cDNA sequences were cloned respectively into the vectors pDH51-GWYFPn (AM779183,
385 to form ETR1-YFPn) and pDH51-GW-YFPc (AM779184, to form PLS-YFPc), and the CTR1
386 cDNA was cloned into pDH51-GW-YFPc (CTR1c), as a control for ETR1 interactions. Intact
387 YFP plasmid was also used as a positive control and YFPc alone was used as a negative control
388 as described previously (*34*). Plasmids were kindly provided by Prof. Don Grierson, University
389 of Nottingham. Transient expression studies following microprojectile bombardment on onion
390 cells. Plasmids were adhered to gold particles to make gold-coated cartridges. 5-10 of these
391 cartridges were used for bombarding onion peel cells. Agar plates containing bombarded onion
392 peels were incubated for 8 hours in dark and then a 1 cm section of the peel was stained with
393 propidium iodide (10 mg/ml) for 1 min and viewed under confocal microscope. Experiments
394 were repeated at least three times.
395
396 **Co-immunoprecipitation**
397 To investigate the interaction between the PLS peptide and the ethylene receptor ETR1, two
398 DNA constructs were created by Gateway cloning. The 105-nucleotide *PLS* gene (without the
399 stop codon) was inserted into the pEarlyGate103 (pEG103) destination vector, containing the
400 *p35S* promoter and a C-terminal GFP tag, producing a vector containing the *p35S::PLS:GFP*
401 DNA. The ETR1 cDNA was inserted into the pEarlyGate301 (pEG301) vector to create a
402 *p35S::ETR1:HA* construct, producing an ETR1 protein with a C-terminal HA tag.
403
404 **Infiltration into *Nicotiana benthamiana***
405 The transient expression of constructs in *Nicotiana benthamiana* (tobacco) leaves was based on
406 a previously published method (*36*). Experiments were replicated up to 5 times. Competent
407 *Agrobacterium tumefaciens* GV3101 cells were transformed with the desired plasmid containing
408 the gene of interest. Individual colonies were used to inoculate liquid LB cultures containing 25
409 µg/ml gentamicin, 50 µg/ml rifampicin and the specific antibiotic required to select for the
410 desired plasmid. The liquid cultures were grown at 28°C for 14-16 h with shaking at 220 rpm.
411 Additionally, liquid cultures of GV3101 containing the p19 protein that is encoded by the tomato
412 bushy plant virus were also prepared in order to suppress post-transcriptional gene silencing (*36*).
413 The overnight cultures were grown until an OD_{600} of approximately 0.6 was reached, and then
414 centrifuged at 3000 x *g* for 5 min. These cells were then twice washed with 10 ml of an infiltration
415 buffer containing 10 mM $MgCl_2.6H_20$, resuspended in 1 ml of the same solution and
416 subsequently incubated at room temperature for 3-5 h. Prior to infiltration, each construct was
417 mixed with p19 and infiltration buffer in a 1:1.2:1.8 ratio.
418 Several small cuts were made with a scalpel on the abaxial surface of the *N. benthamiana*
419 leaves, and were subsequently injected with each of the constructs using a syringe. The plants
420 were approximately 7 to 10 weeks old; the chosen leaves were healthy and of length 3-6 cm, and
421 3 to 4 leaves were infiltrated with each construct.
422
423 **Protein extraction and PLS/ETR1 co-immunoprecipitation**
424 Total protein was extracted from the infiltrated leaves of *N. benthamiana* plants 3 d after
425 infiltration for co-immunoprecipitation (Co-IP/pull-down) experiments to investigate the
426 interaction between PLS and ETR1 proteins.

427 1.5 g of leaf tissue was harvested from each *A. tumefaciens* construct infiltration event, frozen
428 with liquid nitrogen and ground gently using a mortar and pestle. For competition assays, 5 nM
429 or 25 nM full-length PLS peptide was also infiltrated in the presence of 50 µM MG-132 (a
430 proteasome inhibitor) 30 min prior to tissue freezing. The homogenate was transferred to a pre-
431 cooled microcentrifuge tube. 2 ml of extraction buffer was added (20 mM sodium phosphate pH
432 7.4, 100 mM NaCl, 80 mM KCl, 1% glycerol, 0.1 % Triton, 10 mM DTT, plus 1 mini protease
433 inhibitor cocktail tablet, Roche, Switzerland) per 20 ml of extraction buffer, and the extra
434 addition of either 2 mM EDTA or 0.5 µM $CuSO_4$ for binding studies), and the solution was
435 ground further and vortexed until the homogenate was smooth. The solution was centrifuged for
436 12 min at 14000 x *g*, 4°C.
437 ChromoTek (Planegg, Germany) anti-GFP beads were used to immunoprecipitate the PLS-GFP
438 protein, and Sigma-Aldrich (St. Louis, USA) anti-HA beads for the HA-tagged ETR1. 25 µl bead
439 slurry was resuspended in 500 µl ice-cold dilution buffer (20 mM sodium phosphate pH 7.4, 100
440 mM NaCl, 80 mM KCl, 1% glycerol, 0.1 % Triton, 10 mM DTT, plus 1 mini protease inhibitor
441 cocktail tablet) and centrifuged for 2 minutes at 2500 x *g* at 4°C. The supernatant was discarded
442 and the beads were washed twice more with 500 µl ice-cold dilution buffer.
443 The supernatant from the protein sample extraction from *N. benthamiana* plants was mixed
444 with 50 µl GFP beads or HA beads and incubated for 30 minutes at 4°C, mixing every 2 minutes.
445 The mixture was centrifuged at 2500 x *g* for 2 min at 4°C, washed twice with 500 µl ice-cold
446 dilution buffer, and the beads were transferred to a new microcentrifuge tube. The target protein
447 was eluted with the addition of 100 µl 2x SDS sample buffer (120 mM Tris pH 6.8, 50 mM 4%
448 (w/v) SDS, 20% (v/v) glycerol) and the sample was boiled for 10 minutes at 95°C to dissociate
449 immunocomplexes from the beads. The mixture was centrifuged for at 2500 x *g* for 2 minutes at
450 4°C to separate the beads, and the supernatant was transferred to a new microcentrifuge tube.
451 The supernatant was used in SDS-PAGE analysis.
452
453 **Sodium Dodecyl Sulphate Polyacrylamide Gel Electrophoresis (SDS-PAGE)**
454 SDS-PAGE was used to separate protein fragments. The complexed proteins from the pull-down
455 assay were analysed on 10-12% acrylamide gels.
456 Firstly, the resolving gel was prepared by adding the chosen amount of acrylamide (ProtoGel,
457 30% (w/v) acrylamide, 0.8% (w/v) bisacrylamide solution, National Diagnostics) to the resolving
458 buffer (0.1% (w/v) SDS, 375 mM Tris, polymerized via the addition of 0.1% (v/v) ammonium
459 persulphate solution (APS) and finally set by the addition of 1.4 µl/ml TEMED (NNN'N'-
460 tetramethylethylenediamine). The stacking gel was then prepared again by adding the appropriate
461 amount of acrylamide to the stacking buffer (consisting of 0.1% w/v SDS, 125 mM Tris).
462 Polymerization was activated by adding 0.1% (v/v) APS and set using 4 µl/ml TEMED.
463 SDS-PAGE gels were run in a tank containing an electrode buffer (25 mM Tris, 0.1% (v/v)
464 glycerol, 190 mM glycine, diluted 1:10 with dH2O) at 90 V for approximately 90 min. 6 µl
465 PageRuler™ Plus Prestained Protein Ladder, 10 to 250 kDa (ThermoFisher Scientific) was
466 loaded as a protein size marker, displaying coloured bands at 10, 15, 25, 35, 55 70, 100, 130 and
467 250 kDa.
468
469 **Western Blotting**
470 Following electrophoresis, the SDS gels were first washed in 1x transfer buffer (0.04% (w/v)
471 SDS, 20% (v/v) methanol, 38 mM glycine, 48 mM Tris) for 5 minutes. The proteins were then
472 transferred overnight onto nitrocellulose membranes (Whatman, GE Healthcare Life Sciences,
473 Buckinghamshire, UK) in a 1 litre tank containing transfer buffer at 30 V.

The nitrocellulose membranes were incubated in milk buffer (5% (w/v) dried skimmed milk powder (Tesco, Durham, UK), 150 mM NaCl, 10 mM Tris, 0.1% (v/v) Tween 20, pH 7.4) for 20 min to block non-specific protein binding. Following this treatment, the membranes were incubated with primary antibody for 2.5 h (GFP, Abcam, Cambridge, UK: rabbit, 1:10000; HA [Roche], rat, 1:3000). Excess primary antibody was then removed by washing three times in 2x TBST (150 mM NaCl, 10 mM Tris, 0.1% (v/v) Tween 20, pH 7.4) for 2 m, 5 min and 10 min, and subsequently incubated for 1 h with the ECL peroxidase-labelled anti-rabbit or anti-rat IgG secondary antibody, diluted 1:20000 in TBST. Excess secondary antibody was removed again by washing three times in 1x TBST, as with the primary antibody. In order to visualize the probed blot, the membrane was incubated with ECL Western Blotting Detection Reagent immediately prior to imaging. The horseradish peroxidase conjugated to the secondary antibody was detected by using X-ray film, which was subsequently developed in a dark room.

Estimation of synthetic PLS concentration

Freeze-dried synthetic PLS peptide (Cambridge Research Biochemicals, Billingham) was dissolved in DMSO. An aliquot was added to aqueous buffer (10 mM HEPES pH7, 20 mM NaCl, 80 mM KCl) and absorbance at 280 nm was recorded. Concentration was estimated from the absorbance and the ProtParam estimated extinction coefficient of 2,980 M^{-1} cm^{-1}. Concurrent with this a sample was submitted for quantitative amino acid analysis (Abingdon Health Laboratory Services). From this analysis a conversion factor of 2.27 was generated, which was applied to concentrations determined by A280 nm.

ATX1 purification

E. coli BL21(DE3) containing pETatx1 was used to overexpress the wildtype *ATX1* gene from *Arabidopsis thaliana* (optimised for expression in *E. coli*, Novoprolabs). Harvested cells were collected and frozen at -20 ^{o}C overnight then defrosted, resuspended in 20 mM HEPES (pH 7.0), 10 mM EDTA, 100 mM NaCl, 10 mM DTT. Cells were sonicated (Bandelin Sonoplus), supernatant separated by size exclusion chromatography (GE Healthcare, HiLoad 26.600 Superdex 75 pg) metal-free buffer lacking EDTA. Fractions containing ATX1 were incubated overnight and pooled before transfer into an anaerobic chamber (Belle Technology) via desalting column where reductant was removed. ATX1 was quantified by combination of Bradford assay and Ellman's reagent to ensure the fully reduced state of the protein. Samples were also analysed for metal content by ICP-MS to ensure > 95% apo-ATX1.

MBP-PLS/mutant purification

A fusion of PLS to MBP was created using the NEBExpress MBP Fusion and Purification System. Two complementary oligonucleotide primers encoding PLS (optimised for expression in *E. coli*) were annealed and inserted into the pMal-c5x plasmid at XmnI and SalI insertion sites.

The three mutants MBP-PLS(C6S), MBP-PLS(C17S) and MBP-PLS(C6S/C17S) were created by site-directed mutagenesis (QuikChange II, Agilent). *E. coli* NEB Express containing the pMal plasmid with the correct MBP-PLS mutant was used to overexpress each protein. Harvested cells were resuspended in 20 mM Tris-HCl (pH 7.4), 200 mM NaCl, 1 mM EDTA and frozen at -20 ^{o}C overnight. Cells were defrosted in cold H_2O, sonicated, purified by ammonium sulphate precipitation (where MBP-PLS precipitates >60% saturation), separated on MBP-trap (GE Healthcare) and eluted using buffer containing 10 mM maltose. MBP-PLS-containing fractions were pooled and concentrated using centrifugal concentrator (Corning, Spin-X UF 30 KDa) and buffer exchanged by desalting column into metal-free 20 mM HEPES (pH 7.0), 50 mM NaCl buffer in an anaerobic chamber (Belle Technology). Mutants containing thiols were quantified

522 Ellman's assay and MBP-PLS(C6S/C17S), which lacks all thiols, was quantified by Bradford
523 assay alone. Samples were also analysed for metal content by ICP-MS to ensure >95% apo-
524 protein.
525
526 **Anaerobic spectroscopic analysis of Cu(I) complexes**
527 All Cu(I) titration experiments were carried out in an anaerobic chamber (Belle Technology)
528 using metal-free CHELEX-treated, degassed buffers. For experiments titrating Cu(I), aqueous
529 $CuSO_4$ stock was quantified in advance by ICP-MS and diluted to working concentrations. The
530 reductant NH_2OH was included at final concentration of 1 mM to retain Cu(I) in its reduced state.
531 Proteins were diluted in buffer to the final concentration specified in each titration in air-tight
532 quartz cuvettes (Helma), and after addition of probe to the concentration specified, titrated with
533 $CuSO_4$. After each addition, solutions were thoroughly mixed and absorbance spectra recorded
534 using a Lambda 35 UV/Vis spectrophotometer (Perkin Elmer). Titration isotherm data was fitted
535 using simulated affinity curves using Dynafit (*37*).
536
537 **Interaction studies of PLS with copper transporter ETR1 by Microscale Thermophoresis**
538 Fluorescently labelled ETR1 truncation mutants were added to a dilution series of PLS in 50 mM
539 HEPES, 150 mM NaCl, 0.015 % (wv) FosCholine 16 (pH 7.6) or 50 mM Tris, 300 mM NaCl,
540 0.015 % (w/v) FosCholine 16 (pH 7.6). Dissociation constants were calculated using GraphPad
541 Prism 5.
542
543 **Determination of dissociation constants for the PLS-ETR1 interaction**
544 Full-length ETR1 and truncation mutants were purified and labelled as described in (*38*). 94 µM
545 PLS were diluted serially in 50 mM Tris and 300 mM NaCl (pH 7.6). Fluorescently labelled
546 receptor was added at a final concentration of 50 nM. Thermophoretic behaviour was measured
547 in premium capillaries at 50 % LED and 50 % MST power. In case of a binding event, data were
548 fitted using GraphPad Prism 5.
549
550 **Interaction studies of PLS with copper transporter RAN1 and copper chaperones by**
551 **Microscale Thermophoresis**
552 PLS was titrated to fluorescently labelled RAN1 and RAN1 truncation mutants. RAN1,
553 NterRAN1 and CterRAN1 were purified and labelled as described in (*27*). NterRAN1 is a
554 truncation containing only of two N-terminal metal-binding-domains, whereas CterRAN1 is a
555 construct lacking this region. Direct interaction between PLS and RAN1 was observed using
556 Microscale Thermophoresis. Dissociation constants indicate that PLS interacts predominantly
557 with the N-terminal metal-binding-domains, but only weakly with the C-terminal region.
558 Dissociation constants were determined using GraphPad Prism 5. Titration experiments were
559 also carried out with fluorescently labelled copper chaperones ATX, CCH and CCHΔ, a mutant
560 lacking the plant specific C-terminal extension. Proteins were purified and labelled as described
561 (*27*).
562
563 **Ratiometric analysis of roGFP2 fusion proteins**
564 N- and C-terminal roGFP2 fusion proteins of PLS were generated by Gateway cloning.
565 Infiltration and transient expression of roGFP2 fusions and control proteins were carried out as
566 described in (*39*). Image acquisition and data analysis were carried out as described in (*27*). A
567 minimum of 10 leaf optical sections were imaged and used for ratiometric analysis of the redox
568 sensitive excitation properties of roGFP2.
569

570 **Statistical methods**
571 For gene expression analysis and growth assays, a minimum of three biological replicates was
572 used - see Supplementary Materials, Figure legends, Supplementary Table S1, expression data
573 on Dryad (*19*). For protein-protein interaction and protein localization studies, assays were
574 carried out independently between 2 and 10 times (Figs. 2, 3 legends). At least three biological
575 replicates were used for plant growth assays, RNA-seq and gene expression (RT-qPCR)
576 experiments, metal binding assays (Fig. 4). Normalised values from at least three biological
577 replicates were then used for one- or two-way analysis of variance (ANOVA) where appropriate
578 and indicated in relevant Figure legends. Error bars are defined in Figure legends, where relevant.
579
580
581 **References**
582 1. Johnson, P.R., Ecker J.R. The ethylene gas signal transduction pathway: A molecular
583 perspective. *Ann. Rev. Genet.* ***32***, 227-254 (1998).
584
585 2. Chang, C., Kwok, S.F., Bleecker, A.B., Meyerowitz, E.M. Arabidopsis ethylene-response gene
586 *ETR1* - similarity of product to 2-component regulators. *Science* **262**, 539-544 (1993).
587
588 3. Hua, J., Chang, C., Sun, Q., Meyerowitz, E.M. Ethylene insensitivity conferred by
589 Arabidopsis *ERS* gene. *Science* **269**, 1712-1714 (1995).
590
591 4. Hua, J., Sakai, H., Nourizadeh, S., Chen, Q.G., Bleecker, A.B., Ecker, J.R., Meyerowitz, E.M.
592 EIN4 and ERS2 are members of the putative ethylene receptor gene family in Arabidopsis. *Plant*
593 *Cell* **10**, 1321-1332 (1998).
594
595 5. Sakai, H., Hua, J., Chen, Q.G., Chang, C., Medrano, L.J., Bleecker, A.B., Meyerowitz, E.M.
596 *ETR2* is an *ETR1*-like gene involved in ethylene signaling in *Arabidopsis*. *Proc. Natl. Acad. Sci.*
597 *USA* **95**, 5812-5817 (1998).
598
599 6. Chen, Y.F., Randlett, M.D., Findell, J.L., Schaller, G.E. Localization of the ethylene receptor
600 ETR1 to the endoplasmic reticulum of Arabidopsis. *J. Biol. Chem*. **277**, 19861-19866 (2002).
601
602 7. Grefen, C., Staedele, K., Ruzicka, K., Obrdlik, P., Harter, K., Horak, J. Subcellular localization
603 and in vivo interactions of the *Arabidopsis thaliana* ethylene receptor family members. *Molec.*
604 *Plant* **1**, 308-320 (2008).
605
606 8. Schaller, G.E., Ladd, A.N., Lanahan, M.B., Spanbauer, J.M., Bleecker, A.B. The ethylene
607 response mediator ETR1 from Arabidopsis forms a disulfide-linked dimer. *J. Biol. Chem*. **270**,
608 12526-12530 (1995).
609
610 9. Hall, A.E., Findell, J.L., Schaller, G.E., Sisler, E.C., Bleecker, A.B. Ethylene perception by
611 the ERS1 protein in Arabidopsis. *Plant Physiol.* **123**, 1449-1457 (2000).
612
613 10. Rodriguez, F.I., Esch, J.J., Hall, A.E., Binder, B.M., Schaller, G.E., Bleecker, A.B. A copper
614 cofactor for the ethylene receptor ETR1 from Arabidopsis. *Science* **283**, 996-998 (1999).
615

616 11. McDaniel, B.K., Binder, B.M. ETHYLENE RECEPTOR 1 (ETR1) is sufficient and has the
617 predominant role in mediating inhibition of ethylene responses by silver in *Arabidopsis thaliana*.
618 *J. Biol. Chem.* **287**, 26094-26103 (2012).
619
620 12. Chang, C.R. Ethylene signaling: the MAPK module has finally landed. *Trends Plant Sci.* **8**,
621 365-368 (2003).
622
623 13. Gao, Z.Y., Chen, Y.-F., Randlett, M.D., Zhao, X.-C., Findell, J.L., Kieber, J.J., Schaller, G.E.
624 Localization of the Raf-like kinase CTR1 to the endoplasmic reticulum of Arabidopsis through
625 participation in ethylene receptor signaling complexes. *J. Biol. Chem*. **278**, 34725-34732 (2003).
626
627 14. Hirayama, T., Kieber, J.J., Hirayama, N., Kogan, M., Guzman, P., Nourizadek, S., Alonso,
628 J.M., Dailey, W.P., Dancis, A., Ecker, J.R. RESPONSIVE-TO-ANTAGONIST1, a
629 Menkes/Wilson disease-related copper transporter, is required for ethylene signaling in
630 Arabidopsis. *Cell* **97**, 383-393 (1999).
631
632 15. Binder, B.M., Rodriguez, F.I., Bleecker, A.B. The copper transporter RAN1 is essential for
633 biogenesis of ethylene receptors in Arabidopsis. *J. Biol. Chem*. **285**, 37263-37270 (2010).
634
635 16. Qu, X., Hall, B.P., Gao, Z.Y., Schaller, G.E. A strong constitutive ethylene-response
636 phenotype conferred on Arabidopsis plants containing null mutations in the ethylene receptors
637 *ETR1* and *ERS1*. *BMC Plant Biol*. **7**, 3 (2007).
638
639 17. Casson, S.A., Chilley, P.M., Topping, J.F., Evans, I.M., Souter, M.A., Lindsey, K. The
640 *POLARIS* gene of Arabidopsis encodes a predicted peptide required for correct root growth and
641 leaf vascular patterning. *Plant Cell* **14**, 1705-1721 (2002).
642
643 18. Chilley, P.M., Casson, S.A., Tarkowski, P., Hawkins, N., Wang, K.L., Hussey, P.J., Beale,
644 M., Ecker, J.R., Sandberg, G.K., Lindsey, K. The POLARIS peptide of Arabidopsis regulates
645 auxin transport and root growth via effects on ethylene signaling. *Plant Cell* **18**, 3058-3072
646 (2006).
647
648 19. Mudge, A.J., Mehdi, S., Michaels, W., Orosa-Puente, B., Shen, W., Sadanandom, A.,
649 Hetherington, F.M., Hoppen, C., Uzun, B., Groth, G., Topping, J.F., Robinson, N.J., Lindsey, K.
650 Data from: A peptide that regulates metalation of the *Arabidopsis* ethylene receptor. *Dryad*
651 *Digital Repository.* https://doi.org/10.5061/dryad.wpzgmsbss.
652
653 20. Lee, H., Sparkes, I., Gattolin, S., Dzimitrowicz, N., Roberts, L.M., Hawes, C., Frigerio, L.
654 An Arabidopsis reticulon and the atlastin homologue *RHD3-like2* act together in shaping the
655 tubular endoplasmic reticulum. *New Phytol.* **197**, 481-489 (2013).
656
657 21. Bauer, M., Papenbrock, J. Identification and characterization of single-domain thiosulfate
658 sulfurtransferases from Arabidopsis thaliana. *FEBS Lett*. **532**, 427-431 (2002).
659
660 22. Schott-Verdugo, S., Müller, L., Classen, E., Gohlke, H., Groth, G. Structural model of the
661 ETR1 ethylene receptor transmembrane sensor domain. *Sci Rep.* **9,** 8869 (2019).

23. Robinson, N.J., Winge, D.R. Copper metallochaperones. *Ann. Rev. Biochem.* **79**, 537-562 (2010).

24. Xiao, Z., Brose, J., Schimo, S., Ackland, S.M., La Fontaine, S., Wedd, A.G. Unification of the copper(I) binding affinities of the metallo-chaperones Atx1, Atox1, and related proteins: detection probes and affinity standards. *J. Biol. Chem.* **286**, 11047-11055 (2011).

25. Morgan, M.T., Bourassa, D., Harankhedkar, S., McCallum, A.M., Zlatic, S.A. *et al.* Ratiometric two-photon microscopy reveals attomolar copper buffering in normal and Menkes mutant cells. *Proc. Natl. Acad. Sci. USA* **116**, 12167–12172 (2019).

26. Yu, C.H., Yang, N., Bothe, J., Tonelli, M., Nokhrin, S., Dolgova, N. V., *et al.* The metal chaperone Atox1 regulates the activity of the human copper transporter ATP7B by modulating domain dynamics. *J. Biol. Chem.* **292**, 18169 (2017).

27. Hoppen, C., Müller, L., Hänsch, S., Uzun, B., Milic, D., Meyer, A.J., Weidtkamp-Peters, S., Groth, G. Soluble and membrane-bound protein carrier mediate direct copper transport to the ethylene receptor family. *Sci Rep.* **9**, 10715 (2019).

28. Li, W., Lacey, R.F., Ye, Y., Lu, J., Yeh, K.-C., Xiao, Y., Li, L., Wen, C.-K., Binder, B.M., Zhao, Y. Triplin, a small molecule, reveals copper ion transport in ethylene signaling from ATX1 to RAN1. *PLOS Genet.* **13**, e1006703.

29. Liu, J., Mehdi, S., Topping, J., Tarkowski, P., Lindsey, K. Modelling and experimental analysis of hormonal crosstalk in Arabidopsis. *Molec. Systems Biol*. **6**, 373 (2010).

30. Matsuzaki, Y., Ogawa-Ohnishi, M., Mori, A., Matsubayashi, Y. Secreted peptide signals required for maintenance of root stem cell niche in Arabidopsis. *Science* **329**, 1065-1067 (2010).

31. Clough, S.J., Bent, A.F. Floral dip: a simplified method for *Agrobacterium*-mediated transformation of *Arabidopsis thaliana*. *Plant J*. **6**, 735-743 (1998).

32. Thompson, H.L., Shen, W., Matus, R., Kakkar, M., Jones, C., Dolan, D., Grellscheid, S., Yang, X., Zhang, N., Mozaffari-Jovin, S., Chen, C., Zhang, X., Topping, J.F., Lindsey, K. MERISTEM-DEFECTIVE regulates the balance between stemness and differentiation in the root meristem through RNA splicing control. *Development* **150**, dev201476.

33. Love, M.I., Huber, W., Anders, S. Moderated estimation of fold change and dispersion for RNA-seq data with DESeq2. *Genome Biol.* **15**, 550 (2014).

34. Zhong, S., Lin, Z., Grierson, D. Tomato ethylene receptor-CTR interactions: visualization of NEVER-RIPE interactions with multiple CTRs at the endoplasmic reticulum. *J. Exp. Bot.* **59**, 965-972 (2008).

35. Brandizzi, F., Snapp, E.L., Roberts, A.G., Lippincott-Schwartz, J., Hawes, C. Membrane protein transport between the endoplasmic reticulum and the golgi in tobacco leaves is energy dependent but cytoskeleton independent: Evidence from selective photobleaching. *Plant Cell* **14**, 1293-1309 (2002).

36. Voinnet, O., Rivas, S., Mestre, P., Baulcombe, D. An enhanced transient expression system in plants based on suppression of gene silencing by the p19 protein of tomato bushy stunt virus. *Plant J*. **33**, 949-956 (2003).

37. Kuzmič, P. DynaFit—A Software Package for Enzymology. *Meth. Enzymol*. **467**, 247–280 (2009).

38. Milić, D., Dick, M., Mulnaes, D., Pfleger, C., Kinnen, A., Gohlke, H. *et al.*, Recognition motif and mechanism of ripening inhibitory peptides in plant hormone receptor ETR1. *Sci. Rep.* **8**, 1–12 (2018).

39. Brach, T., Soyk, S., Mueller, C., Hinz, G., Hell, R., Brandizzi, F., Meyer, A.J. Non-invasive topology of membrane proteins in the secretory pathway. *Plant J.* **57**, 534-541 (2009).

Acknowledgements: We thank Prof. Steven Cobb (Durham University Department of Chemistry) for advice on peptide synthesis, and Dr. Andrew Foster (Durham University Department of Chemistry) for preliminary peptide-Cu interaction analysis. The authors acknowledge financial support from: UK Biotechnology and Biological Sciences Research Council BB/E006531/1, BBS/B/0773X, BB/J014516/1 (KL), BB/V006002/1, BB/M011186/1 (NJR); Deutsche Forschungsgemeinschaft (German Research Foundation) 267205415 – SFB 1208 project B06 (GG).

Author contributions:
KL and NJR initiated the project. KL, JFT, NJR, AS and GG designed and supervised aspects of the project. AJM, SM, WM, BO-P, WS, FMH, CH and BU carried out the experimental work and prepared the Figures. KL, NJR and GG drafted the early version of the manuscript, and all authors reviewed and edited the manuscript.

Competing interests: Authors declare no competing interests.

Additional information

Supplementary information The online version contains supplementary materials and RNA-seq and root assay data are available at the Dryad Digital Repository (https://doi.org/10.5061/dryad.wpzgmsbss).

Correspondence and requests for materials should be addressed to Keith Lindsey or Nigel Robinson.

Figure Legends

Figure 1. The PLS peptide is required for ethylene control of seedling growth, is structurally and functionally conserved, and complements the *Arabidopsis pls* mutant.
(**a**). Amino acid sequence of the PLS peptide from *Arabidopsis thaliana* with *Camelina sativa* PLS sequence (*C.s* PLS), and synthetic truncations N1, N2, C1 and C2, indicated by horizontal lines. Two cysteine residues are highlighted in bold. (**b**) Wildtype (left) and *pls* mutant (right); bar = 5 mm. (**c**) Expression levels of 24 ethylene-responsive genes in *pls* and *PLS* overexpressing

seedlings, compared to wildtype levels. (**d**) Effect of *Arabidopsis* PLS full length peptide, *A.t.* PLS(FL), and *Camelina* PLS peptide (*C.s.* PLS) on *Arabidopsis* primary root length. Wildtype (C24) and *pls* mutant seedlings were grown hydroponically in the presence (100 nM) or absence of peptide for 10 d. Asterisks: ANOVA, $F_{2, 41} = 6.86$, $p = 0.003$; Tukey's HSD test. (**e**) Effect of PLS full length and truncated peptides on *Arabidopsis* primary root length. Seedlings were grown hydroponically in the presence of 50 nM peptide for 10 d. C1 = C-terminal 14 amino acids, C2 = C-terminal 24 amino acids, N1 = N-terminal 22 amino acids, N2 = N-terminal 9 amino acids, full length PLS = 36 amino acids. Asterisks: ANOVA, $F_{5,112} = 6.13$, $p = 4.65E-5$). Error bars show ± 1 standard error, n = 14-22.

Figure 2. PLS localizes to the endoplasmic reticulum.
(**a-o**) PLS::PLS:GFP fusion protein (**a, g, j**) colocalizes with endoplasmic reticulum markers ER Tracker (**b, c, c inset**) and RFP:HDEL (**h, i, i inset**), but free GFP does not (**d-f**, **m-o**). PLS:GFP staining is seen also in nuclei (n). PLS::PLS:GFP (**j**) does not co-localize with the *trans*-Golgi markers ST-mCherry SH:GFP (**k, l**). Scale bars = 25 µm (**c, l**), 10 µm (**f, i, o**). (**p**) Ratiometric analysis of roGFP2 fusion constructs transiently expressed in *N. benthamiana*. Comparison of excitation ratios of PLS-roGFP2 and roGFP2-PLS with control constructs (free roGFP, SEC22 fusions) reveals that PLS localizes to the cytosolic side of the ER.

Figure 3. PLS interacts with the ethylene receptor ETR1.
(**a**) Co-immunoprecipitation of PLS:GFP by ETR1:HA (upper panel) in leaves of *Nicotiana benthamiana*, in the presence and absence of 0.5 µM $CuSO_4$ and EDTA (to remove Cu). Lower panel shows presence of ETR1:HA in extracts using anti-HA antibody. (**b**) Densitometric scan of immunoblot. (**c**) Competition assay showing a reduced binding between PLS:GFP and ETR1:HA in the presence of 0, 5 nM or 25 nM PLS peptide, in the presence of 0.5 µM $CuSO_4$ and 50 µM MG-132, a proteasome inhibitor (upper panel). Lower panel shows ETR1:HA in extracts using anti-HA antibody. (**d**) Densitometric scan of immunoblot. (**e**) Co-immunopreciptation of ETR1:HA (upper panel) in leaves of *N. benthamiana*, showing the effect of EDTA (to remove Cu) on interaction between ERT1:HA and PLS:GFP. Lower panel shows presence of ETR1:HA in extracts using anti-HA antibody (**f**) Densitometric scan of immunoblot. α-GFP, anti-GFP antibody; α-HA, anti-HA antibody. (**g**) Microscale thermophoresis binding curves of different ETR1 truncations with PLS. Binding of PLS was observed with full-length ETR1 and all C-terminal truncations but not with $ETR1^{306-738}$ lacking the N-terminal transmembrane part of the receptor.

Figure 4. PLS binds copper and interacts with RAN1 and copper chaperones.
(**a**) C6S and C17S in PLS are required for function. Seedlings were grown hydroponically for 10 d in the presence (100 nM) or absence of peptide (FL or C6S, C17S). Asterisk: ANOVA, $F_{2, 51} = 9.48$, $p = 3.15E-4$, Tukey's HSD). Error bars show ± 1 standard error, n = 14-22. Blue bars are C24, red bars are *pls*. (**b**) Effect of exogenous Cu(I) chelator BCS on primary root length of *Arabidopsis* grown hydroponically for 10 d. Asterisks: Student's t test analysis, $p < 0.005$. Error bars show ±1 standard error. (**c**) Absorption of BCA (17.3 µM) titrated with Cu(I) (representative spectrum, n = 2, full dataset Fig S1). (**d**) Binding isotherms ($A_{358\ nm}$) of BCA (10 µM) in the presence/absence (filled/empty symbols, respectively) of 14 µM MBP-PLS (circles) or MBP-PLS mutants (C6S, C17S and C6S/C17S: triangles, diamonds and squares respectively) titrated with Cu(I) (n = 3, ±SD). (**e**) Binding isotherms ($A_{358\ nm}$) of BCA (50 µM) in the presence/absence of 10 µM MBP-PLS (filled/empty symbols, respectively) titrated with Cu(I). Model (solid line) describes Cu(I)-binding as a 2:1 complex, with β_2 affinity of 3.79 (±1.5) $x10^{19}$ M^{-2}. Dotted lines

804 simulate 10x weaker or tighter affinity (n = 3, ±SD). (**f**) Simulated Cu(I) occupancy
805 (Supplementary Text) as a function of [PLS] using β_2 Cu(I) affinity of 3.79 x10^{19} M^{-2}. Inset,
806 *Arabidopsis* ATX1 (20 μM, filled circles) withholds one Cu(I) equivalent from 20 μM BCA
807 (open circles, BCA-alone) (n = 3, ±SD), with K_D Cu(I) 5.47 x10^{-18} M (Fig. S3). (**g**) Microscale
808 thermophoresis binding curves of copper transporter RAN1 with PLS. (**h**) Microscale
809 thermophoresis binding curves of soluble copper chaperones ATX1 and CCH with PLS (n = 3,
810 ±SD).
811
812

Fig. 1

a

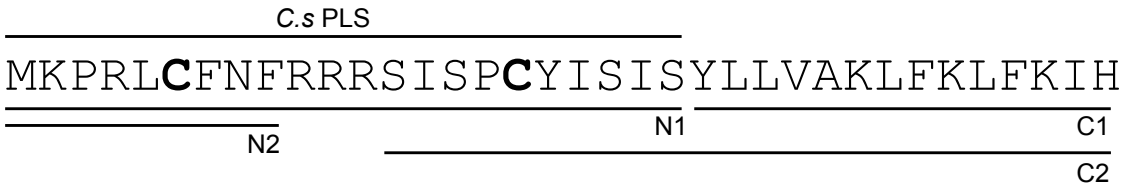
C.s PLS
MKPRLCFNFRRRSISPCYISISYLLVAKLFKLFKIH
N2
N1
C1
C2

b

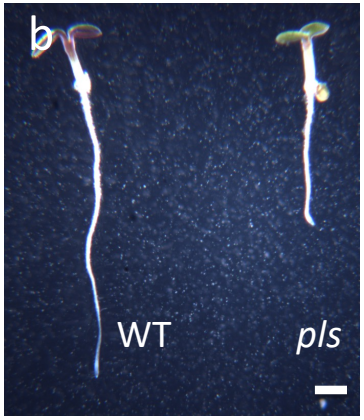
WT
pls

c

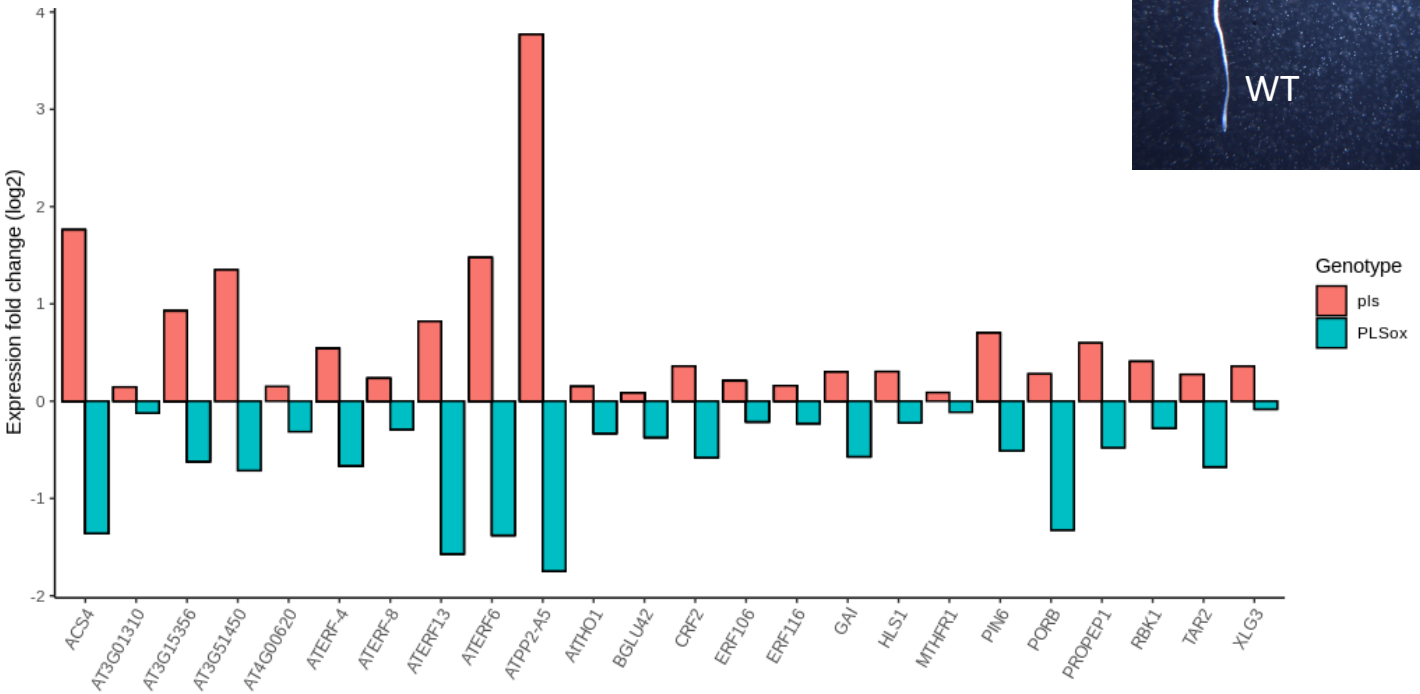
Expression fold change (log2)
4
3
2
1
0
-1
-2
ACS4
AT3G01310
AT3G15356
AT3G51450
AT4G00620
ATERF-4
ATERF-8
ATERF13
ATERF6
ATPP2-A5
AtTHO1
BGLU42
CRF2
ERF106
ERF116
GAI
HLS1
MTHFR1
PIN6
PORB
PROPEP1
RBK1
TAR2
XLG3
Genotype
pls
PLSox

d

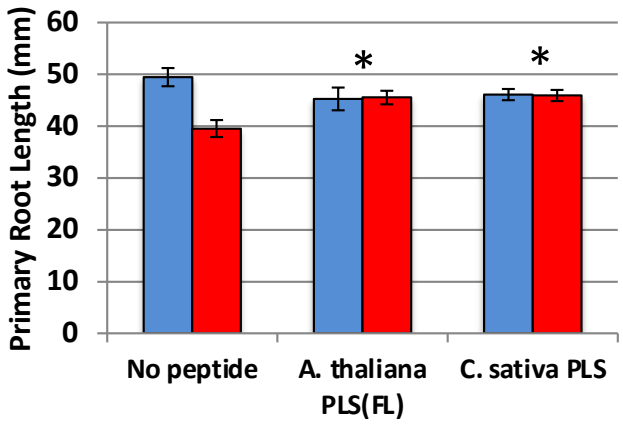
Primary Root Length (mm)
60
50
40
30
20
10
0
*
*
No peptide
A. thaliana PLS(FL)
C. sativa PLS

e

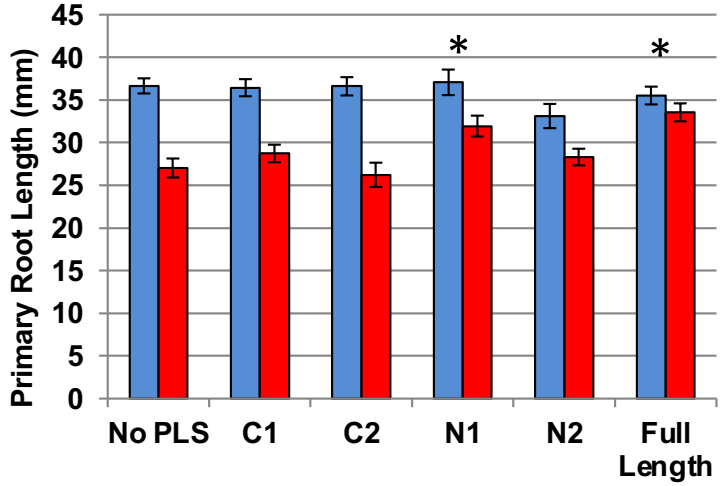
Primary Root Length (mm)
45
40
35
30
25
20
15
10
5
0
*
*
No PLS
C1
C2
N1
N2
Full Length

Figure 1. The PLS peptide is required for ethylene control of seedling growth, is structurally and functionally conserved, and complements the *Arabidopsis pls* mutant.

(**a**). Amino acid sequence of the PLS peptide from *Arabidopsis thaliana* with *Camelina sativa* PLS sequence (*C.s* PLS), and synthetic truncations N1, N2, C1 and C2, indicated by horizontal lines. Two cysteine residues are highlighted in bold. (**b**) Wildtype (left) and *pls* mutant (right); bar = 5 mm. (**c**) Expression levels of 24 ethylene-responsive genes in *pls* and *PLS* overexpressing seedlings, compared to wildtype levels. (**d**) Effect of *Arabidopsis* PLS full length peptide, *A.t.* PLS(FL), and *Camelina* PLS peptide (*C.s.* PLS) on *Arabidopsis* primary root length. Wildtype (C24) and *pls* mutant seedlings were grown hydroponically in the presence (100 nM) or absence of peptide for 10 d. Asterisks: ANOVA, $F_{2,41} = 6.86$, $p = 0.003$; Tukey's HSD test. (**e**) Effect of PLS full length and truncated peptides on *Arabidopsis* primary root length. Seedlings were grown hydroponically in the presence of 50 nM peptide for 10 d. C1 = C-terminal 14 amino acids, C2 = C-terminal 24 amino acids, N1 = N-terminal 22 amino acids, N2 = N-terminal 9 amino acids, full length PLS = 36 amino acids. Asterisks: ANOVA, $F_{5,112} = 6.13$, $p = 4.65E-5$). Error bars show $\pm$ 1 standard error, n = 14-22.

Fig. 2

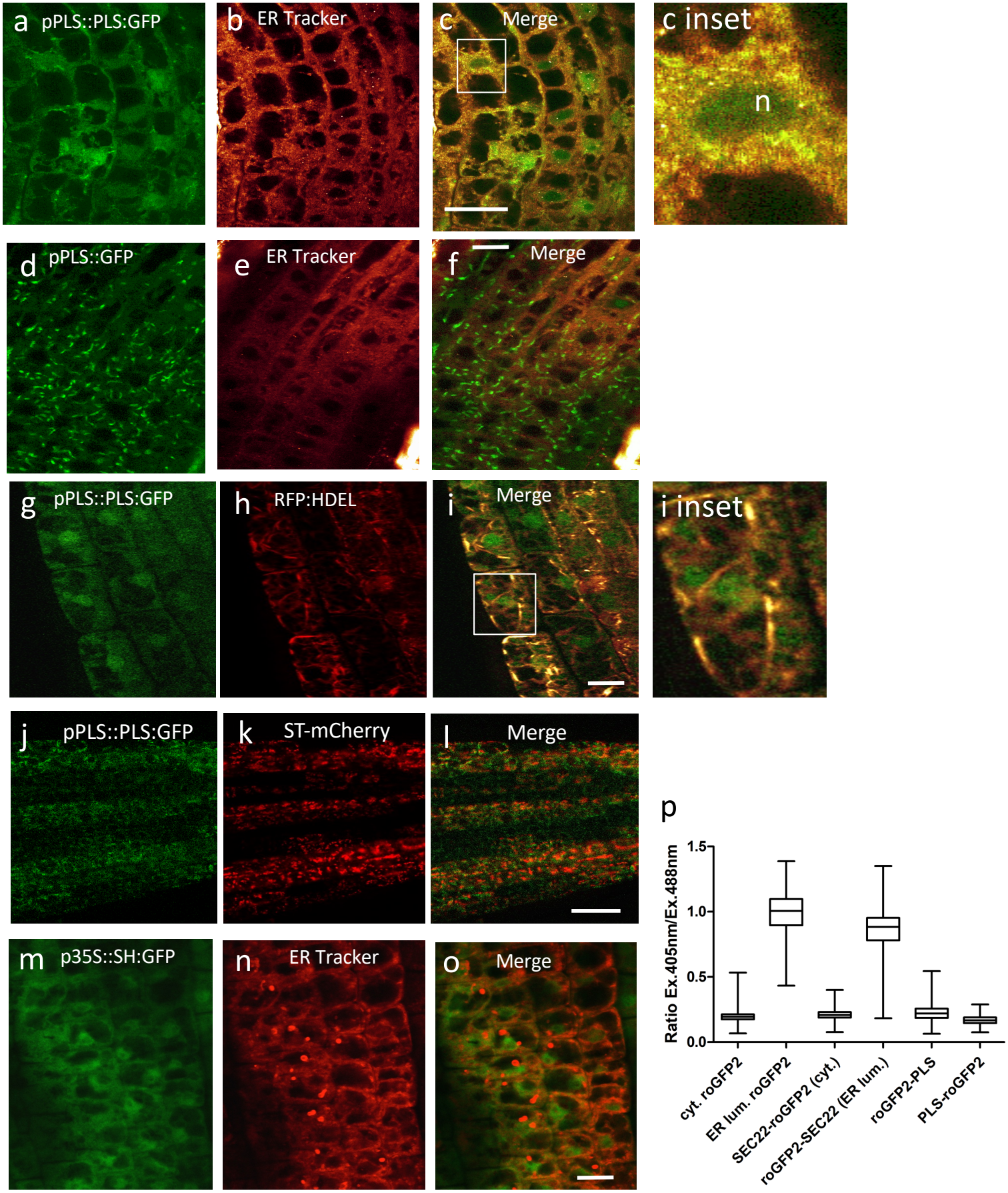
a pPLS::PLS:GFP
b ER Tracker
c Merge
c inset
n
d pPLS::GFP
e ER Tracker
f Merge
g pPLS::PLS:GFP
h RFP:HDEL
i Merge
i inset
j pPLS::PLS:GFP
k ST-mCherry
l Merge
m p35S::SH:GFP
n ER Tracker
o Merge
p
Ratio Ex.405nm/Ex.488nm
1.5
1.0
0.5
0.0
cyt. roGFP2
ER lum. roGFP2
SEC22-roGFP2 (cyt.)
roGFP2-SEC22 (ER lum.)
roGFP2-PLS
PLS-roGFP2

Figure 2. PLS localizes to the endoplasmic reticulum.
(**a-o**) PLS::PLS:GFP fusion protein (**a, g, j**) colocalizes with endoplasmic reticulum markers ER Tracker (**b, c, c inset**) and RFP:HDEL (**h, i, i inset**), but free GFP does not (**d-f**, **m-o**). PLS:GFP staining is seen also in nuclei (n). PLS::PLS:GFP (**j**) does not co-localize with the *trans*-Golgi markers ST-mCherry SH:GFP (**k, l**). Scale bars = 25 μm (**c, l**), 10 μm (**f, i, o**). (**p**) Ratiometric analysis of roGFP2 fusion constructs transiently expressed in *N. benthamiana*. Comparison of excitation ratios of PLS-roGFP2 and roGFP2-PLS with control constructs (free roGFP, SEC22 fusions) reveals that PLS localizes to the cytosolic side of the ER.

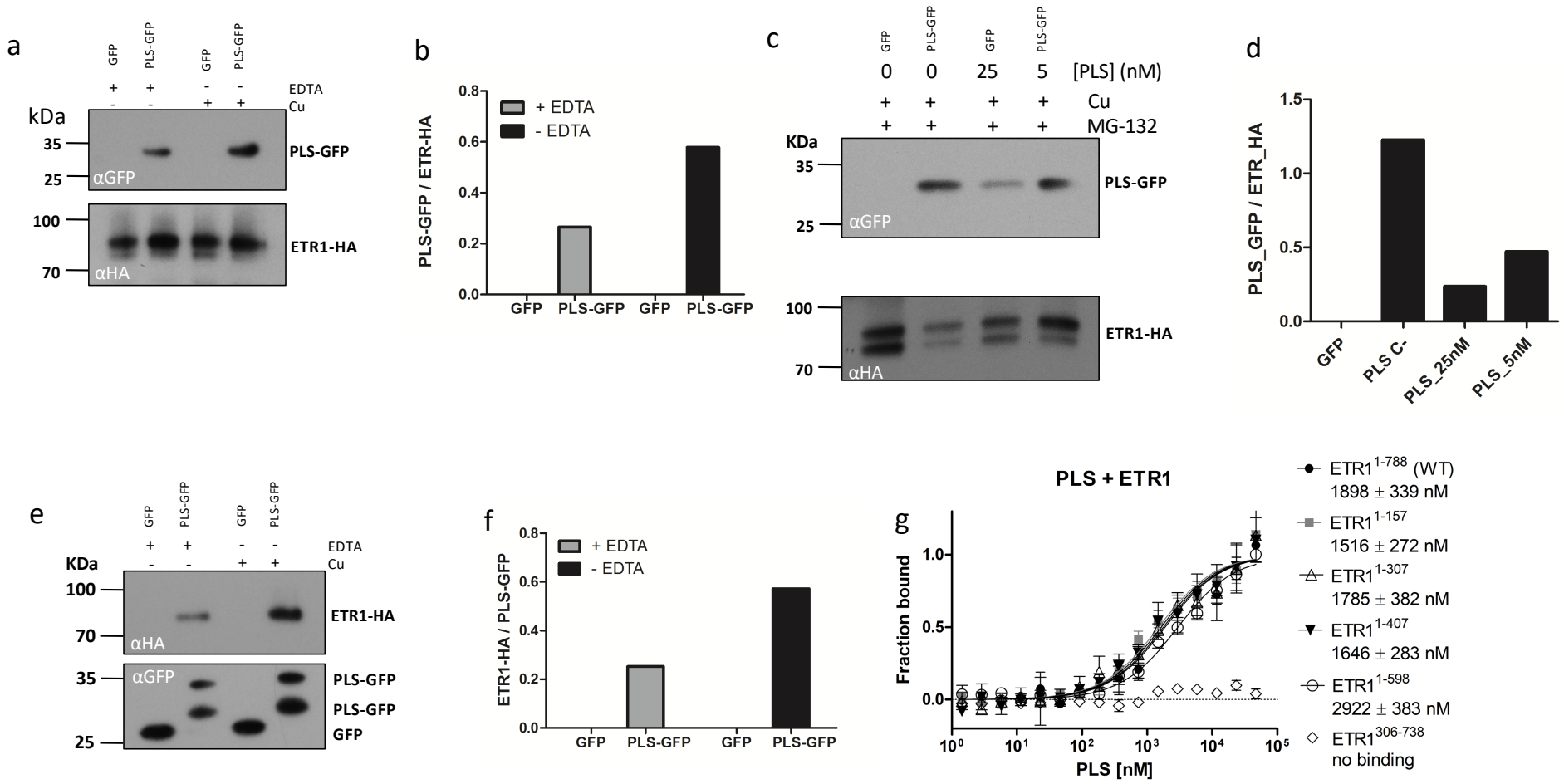
a
GFP
PLS-GFP
GFP
PLS-GFP
EDTA
Cu
kDa
35
25
αGFP
PLS-GFP
100
70
αHA
ETR1-HA
b
PLS-GFP / ETR-HA
+ EDTA
- EDTA
GFP
PLS-GFP
GFP
PLS-GFP
c
0
0
25
5
[PLS] (nM)
Cu
MG-132
KDa
35
25
αGFP
PLS-GFP
100
70
αHA
ETR1-HA
d
PLS_GFP / ETR_HA
GFP
PLS C-
PLS_25nM
PLS_5nM
e
GFP
PLS-GFP
GFP
PLS-GFP
EDTA
Cu
KDa
100
70
αHA
ETR1-HA
35
25
αGFP
PLS-GFP
PLS-GFP
GFP
f
ETR1-HA / PLS-GFP
+ EDTA
- EDTA
GFP
PLS-GFP
GFP
PLS-GFP
g
PLS + ETR1
Fraction bound
PLS [nM]
ETR1 1-788 (WT)
1898 ± 339 nM
ETR1 1-157
1516 ± 272 nM
ETR1 1-307
1785 ± 382 nM
ETR1 1-407
1646 ± 283 nM
ETR1 1-598
2922 ± 383 nM
ETR1 306-738
no binding

Fig. 3

Figure 3. PLS interacts with the ethylene receptor ETR1.

(**a**) Co-immunoprecipitation of PLS:GFP by ETR1:HA (upper panel) in leaves of *Nicotiana benthamiana*, in the presence and absence of 0.5 μM $CuSO_4$ and EDTA (to remove Cu). Lower panel shows presence of ETR1:HA in extracts using anti-HA antibody. (**b**) Densitometric scan of immunoblot. (**c**) Competition assay showing a reduced binding between PLS:GFP and ETR1:HA in the presence of 0, 5 nM or 25 nM PLS peptide, in the presence of 0.5 μM $CuSO_4$ and 50 μM MG-132, a proteasome inhibitor (upper panel). Lower panel shows ETR1:HA in extracts using anti-HA antibody. (**d**) Densitometric scan of immunoblot. (**e**) Co-immunopreciptation of ETR1:HA (upper panel) in leaves of *N. benthamiana*, showing the effect of EDTA (to remove Cu) on interaction between ERT1:HA and PLS:GFP. Lower panel shows presence of ETR1:HA in extracts using anti-HA antibody (**f**) Densitometric scan of immunoblot. α-GFP, anti-GFP antibody; α-HA, anti-HA antibody. (**g**) Microscale thermophoresis binding curves of different ETR1 truncations with PLS. Binding of PLS was observed with full-length ETR1 and all C-terminal truncations but not with $ETR1^{306-738}$ lacking the N-terminal transmembrane part of the receptor.

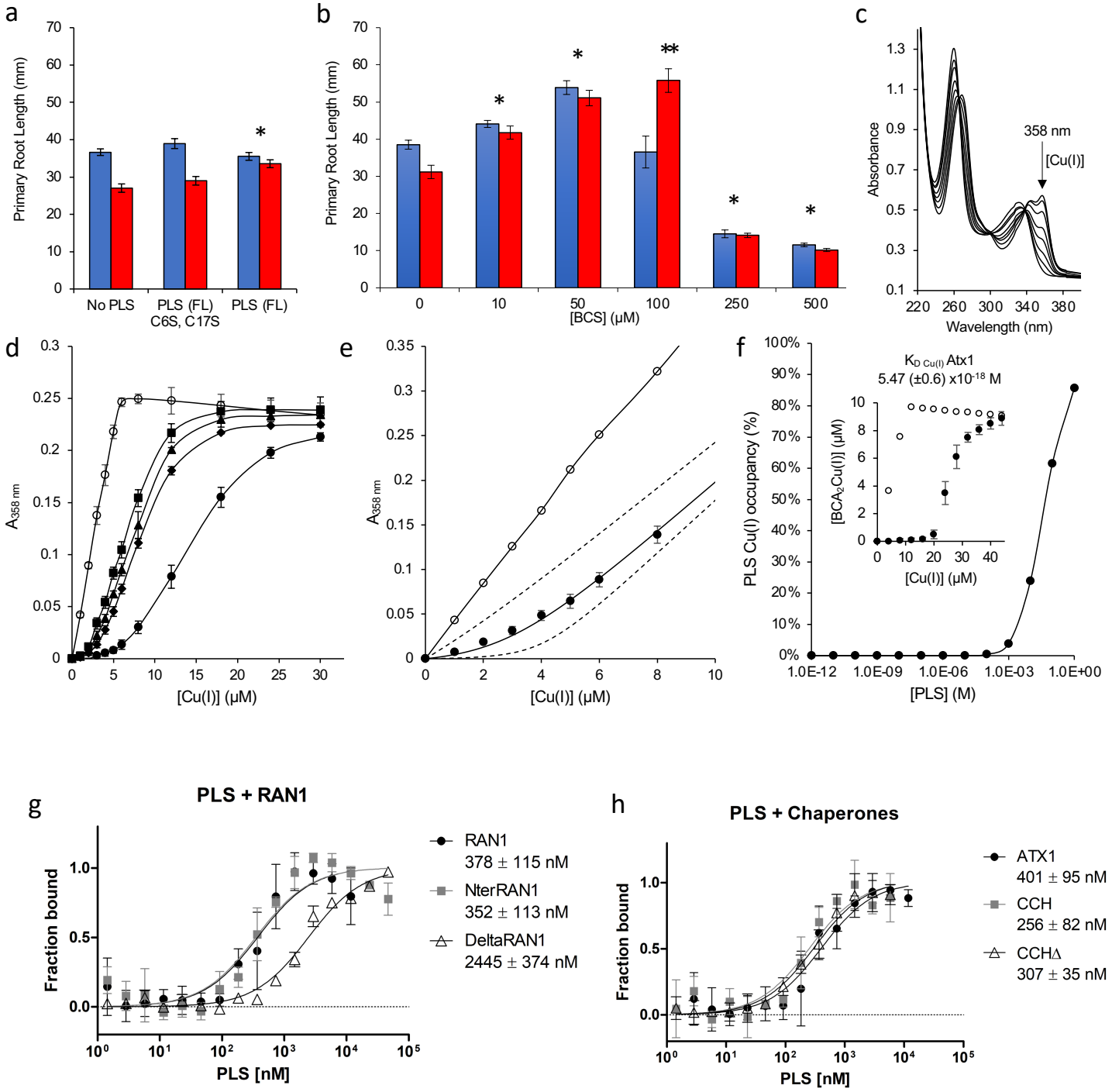
a
Primary Root Length (mm)
No PLS
PLS (FL) C6S, C17S
PLS (FL)
b
Primary Root Length (mm)
[BCS] (μM)
c
Absorbance
358 nm
[Cu(I)]
Wavelength (nm)
d
$A_{358\ nm}$
[Cu(I)] (μM)
e
$A_{358\ nm}$
[Cu(I)] (μM)
f
PLS Cu(I) occupancy (%)
$K_{D\ Cu(I)}$ Atx1
5.47 (±0.6) x10^{-18} M
[BCA$_2$Cu(I)] (μM)
[Cu(I)] (μM)
[PLS] (M)
g
PLS + RAN1
Fraction bound
PLS [nM]
RAN1
378 ± 115 nM
NterRAN1
352 ± 113 nM
DeltaRAN1
2445 ± 374 nM
h
PLS + Chaperones
Fraction bound
PLS [nM]
ATX1
401 ± 95 nM
CCH
256 ± 82 nM
CCHΔ
307 ± 35 nM

Fig. 4

Figure 4. PLS binds copper and interacts with RAN1 and copper chaperones.

(**a**) C6S and C17S in PLS are required for function. Seedlings were grown hydroponically for 10 d in the presence (100 nM) or absence of peptide (FL or C6S, C17S). Asterisk: ANOVA, $F_{2, 51} = 9.48$, $p = 3.15E-4$, Tukey's HSD). Error bars show ± 1 standard error, n = 14-22. Blue bars are C24, red bars are *pls*. (**b**) Effect of exogenous Cu(I) chelator BCS on primary root length of *Arabidopsis* grown hydroponically for 10 d. Asterisks: Student's t test analysis, $p < 0.005$. Error bars show ±1 standard error. (**c**) Absorption of BCA (17.3 μM) titrated with Cu(I) (representative spectrum, n = 2, full dataset Fig S1). (**d**) Binding isotherms ($A_{358\ nm}$) of BCA (10 μM) in the presence/absence (filled/empty symbols, respectively) of 14 μM MBP-PLS (circles) or MBP-PLS mutants (C6S, C17S and C6S/C17S: triangles, diamonds and squares respectively) titrated with Cu(I) (n = 3, ±SD). (**e**) Binding isotherms ($A_{358\ nm}$) of BCA (50 μM) in the presence/absence of 10 μM MBP-PLS (filled/empty symbols, respectively) titrated with Cu(I). Model (solid line) describes Cu(I)-binding as a 2:1 complex, with β_2 affinity of 3.79 (±1.5) $x10^{19}$ M^{-2}. Dotted lines simulate 10x weaker or tighter affinity (n = 3, ±SD). (**f**) Simulated Cu(I) occupancy (Supplementary Text) as a function of [PLS] using β_2 Cu(I) affinity of 3.79 $x10^{19}$ M^{-2}. Inset, *Arabidopsis* ATX1 (20 μM, filled circles) withholds one Cu(I) equivalent from 20 μM BCA (open circles, BCA-alone) (n = 3, ±SD), with K_D Cu(I) 5.47 $x10^{-18}$ M (Fig. S3). (**g**) Microscale thermophoresis binding curves of copper transporter RAN1 with PLS. (**h**) Microscale thermophoresis binding curves of soluble copper chaperones ATX1 and CCH with PLS (n = 3, ±SD).